Proteome-wide cross-linking mass spectrometry to identify specific virus capsid-host interactions between tick-borne encephalitis virus and neuroblastoma cells

Sarah V. Barrass[1,2], Lauri I. A. Pulkkinen[1,2], Olli Vapalahti[3,4,5], Suvi H. Kuivanen[3] ,Maria Anastasina[1,2*], Lotta Happonen[6*], Sarah J. Butcher[1,2*]

[1] Faculty of Biological and Environmental Sciences, Molecular and Integrative Bioscience Research Programme, University of Helsinki, Helsinki, Finland

[2] Helsinki Institute of Life Sciences-Institute of Biotechnology, University of Helsinki, Helsinki, Finland

[3] Department of Virology, University of Helsinki, Helsinki, Finland

[4] Department of Veterinary Biosciences, Faculty of Veterinary Medicine, University of Helsinki, Helsinki, Finland

[5] Division of Clinical Microbiology, University of Helsinki and Helsinki University Hospital, Helsinki, Finland

[6] Lund University, Faculty of Medicine, Department of Clinical Sciences Lund, Infection Medicine, Lund, Sweden

* Corresponding authors

Emails: sarah.butcher@helsinki.fi (SB), lotta.happonen@med.lu.se (LH), maria.anastasina@helsinki.fi (MA)

Abstract

Virus-host protein-protein interactions are central to viral infection, but are challenging to identify and characterise, especially in complex systems involving intact viruses and cells. In this work, we demonstrate a proteome-wide approach to identify virus-host interactions using chemical cross-linking coupled with mass spectrometry. We adsorbed tick-borne encephalitis virus onto metabolically-stalled neuroblastoma cells, covalently cross-linked interacting virus-host proteins, and performed limited proteolysis to release primarily the surface-exposed proteins for identification by mass spectrometry. Using the intraviral protein cross-links as an internal control to assess cross-link confidence levels, we identified 22 high confidence unique intraviral cross-links and 59 high confidence unique virus-host protein-protein interactions. The identified host proteins were shown to interact with eight distinct sites on the outer surface of the virus. Notably, we identified an interaction between the substrate-binding domain of heat shock protein family A member 5, an entry receptor for four related flaviviruses, and the hinge region of the viral envelope protein. We also identified host proteins involved in endocytosis, cytoskeletal rearrangement, or located in the cytoskeleton, suggesting that entry mechanisms for tick-borne encephalitis virus could include both clathrin-mediated endocytosis and macropinocytosis. Additionally, cross-linking of the viral proteins showed that the capsid protein forms dimers within tick-borne encephalitis virus, as previously observed with purified C proteins for other flaviviruses. This method enables the identification and mapping of transient virus-host interactions, under near-physiological conditions, without the need for genetic manipulation.

Author summary

Tick-borne encephalitis virus is an important human pathogen that can cause severe infection often resulting in life-long neurological complications or even death. As with other viruses, it fully relies on the host cells, and any successful infection starts with interactions between the viral structural proteins and cellular surface proteins. Mapping these interactions is essential both for the fundamental understanding

of viral entry mechanisms, and for guiding the design of new antiviral drugs and vaccines. Here, we stabilise the interactions between tick-borne encephalitis virus and human proteins by chemical cross-linking. We then detect the interactions using mass spectrometry and analyse the data to identify protein-protein complexes. We demonstrate that we can visualise the protein interaction interfaces by mapping the cross-linked sites onto the host and viral protein structures. We reveal that there are eight distinct sites on the outer surface of the viral envelope protein that interact with host. Using this approach, we mapped interactions between the tick-borne encephalitis virus envelope protein, and 59 host proteins, identifying a possible new virus receptor. These results highlight the potential of chemical cross-linking coupled with mass spectrometry to identify and map interactions between viral and host proteins.

Introduction

Viruses are obligatory intracellular parasites that depend on virus-host protein-protein interactions (PPIs) to establish successful infections. The identification of these interactions and knowledge of the interaction interfaces contribute to our understanding of the initial steps of the viral life cycle, and can guide the design of antivirals and vaccines [1–6].

Advances in high throughput methods have led to the large-scale identification of virus-host interactions, but the structural characterisation of these interactions is often still limited [7]. Affinity purification coupled with mass spectrometry, yeast two-hybrid, and protein microarrays, have identified virus-host PPIs for multiple viruses including: Japanese encephalitis virus, H1N1 influenza, human immunodeficiency virus, human cytomegalovirus, and severe acute respiratory syndrome coronavirus 2 [8–12]. These methods are however limited in their applicability to detect transient interactions between wild-type viruses and cells. Alternative methods, using chemical cross-linking, or proximity labelling (BioID and TurboID), demonstrate improved detection of weak and transient interactions [13–17]. In these approaches, cells are probed with modified viral proteins conjugated to trifunctional cross-linkers or biotin ligases. Host proteins in close proximity to the viral bait are then permanently cross-linked or biotinylated, and purified using the biotin or cross-linker tag. Enriched proteins are detected by comparison of the protein signal to that in negative

68 controls using bottom-up proteomics. Alternative chemical cross-linking mass spectrometry (XL-MS)
69 workflows that directly detect the cross-linked peptides additionally provide information about the
70 interaction interfaces. Previous studies have used the finite length of the chemical cross-linker to indicate
71 the proximity of two amino acid side chains during the cross-linking reaction, and to build structural models
72 of bacteria-host PPIs [18,19]. This shows the potential of XL-MS in both the identification of PPIs and the
73 characterisation of the binding interface.

74 The flavivirus, tick-borne encephalitis virus (TBEV) is the causative agent of one of the most important
75 arbovirus-caused diseases in Europe, Russia, and Northern China [20,21]. Symptomatic infection with TBEV
76 can cause meningitis, encephalitis, and meningoencephalitis, and often results in life-long neurological
77 complications or death [22,23]. The TBEV virion has three different structural proteins, the envelope
78 protein (E protein), membrane protein (M protein) and capsid protein (C protein), in addition to a lipid
79 bilayer and an ~11 kilobase-long positive-strand RNA genome (Fig 1). The E protein forms the smooth outer
80 surface of the virion and is responsible for receptor binding [25,26]. The atomic structure of the mature
81 TBEV virion E and M proteins has been solved by cryo-electron microscopy at a resolution of 3.9 Å and the
82 crystal structure of the E protein at a resolution of 1.9 Å (Fig 1) [24,25]. Non-infectious immature and
83 partially immature viruses also egress from cells, and have a spikey surface (Fig 1) [24]. No proteome-wide
84 study of TBEV virus-host protein interactions has been published to our knowledge.

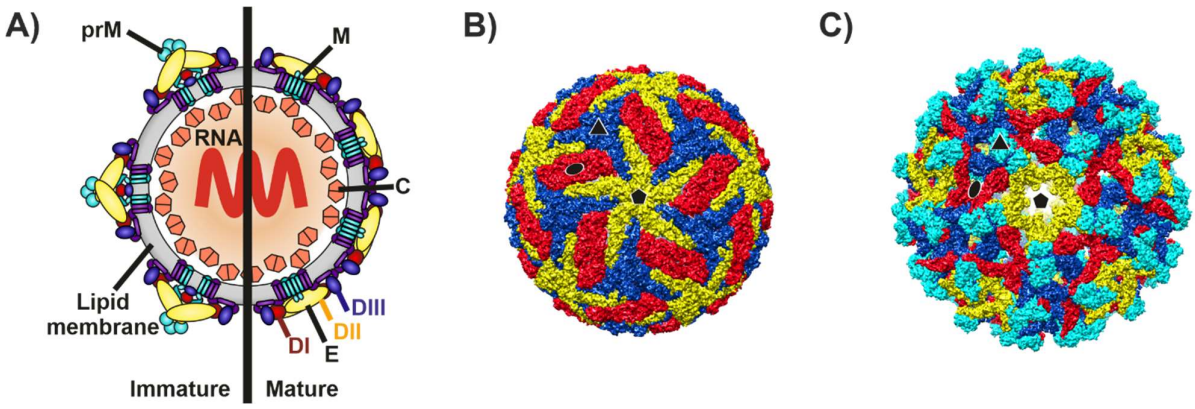

85

86 ***Fig 1: TBEV mature and immature virus structures.*** *A) Schematic representation of TBEV with the*
87 *immature structure shown on the left and the mature on the right. Multiple copies of the C protein dimer*

88 *surround the genome forming the nucleocapsid complex, positioned beneath the lipid bilayer. The surface of*
89 *the immature virion is covered in 60 spikes, composed of trimers of prM (pre-membrane)-E heterodimers*
90 *embedded into the lipid bilayer. The surface of the mature virion is covered in 90 E-M heterotetramer*
91 *complexes embedded into the lipid bilayer. TBEV E protein domain I is shown in red, domain III in dark blue,*
92 *domain II in yellow and domain 4 in purple. B) Surface representation of the mature TBEV virion (PDB*
93 *accession: 5O6A)[24]. The three E proteins within each asymmetric unit are shown in blue, red, and yellow.*
94 *Symmetry axes are indicated by the black pentagon (five-fold), triangle (three-fold), and ellipse (two-fold).*
95 *C) Surface representation of the immature Spondweni virus, a related flavivirus (PDB accession 6ZQW) [27].*
96 *The three E proteins within each asymmetric unit are shown in blue, red, and yellow, and the prM protein is*
97 *shown in cyan. Symmetry axes are indicated by a black pentagon (five-fold), triangle (three-fold), and ellipse*
98 *(two-fold).*

99 In this large-scale proteomics study, we used XL-MS to identify the interaction interfaces of PPIs between
100 TBEV and the surface of human neuroblastoma (SK-N-SH) cells. Here, the homobifunctional chemical cross-
101 linker disuccinimidyl suberate (DSS) was used to covalently fix PPIs by cross-linking primary amine
102 containing residues (the side chain of lysine residues or the N-terminus of the protein). The finite length of
103 DSS (11.4 Å) imposed a maximum distance between cross-linked residues and was used to validate
104 intraviral crosslinks by measuring their distances on TBEV proteins with known structures or reliable
105 homology models. The final dataset was filtered using the intraviral cross-links as an internal control,
106 leading to the identification 59 unique high confidence interactions between the TBEV E protein and
107 cellular proteins.

108 # Results

109 ## Identification of cross-linked peptides

110 To identify interactions between the mature TBEV virion and host proteins, we incubated the virus with
111 metabolically-stalled neuroblastoma cells on ice, allowing for TBEV to bind to the cells, but preventing

112 subsequent internalization. The TBEV-host PPIs were then stabilized and fixed by chemical cross-linking
113 with DSS (Fig 2). To reduce the sample complexity and search space during data analysis, we used limited
114 proteolysis to release primarily cell-surface associated host proteins. The released proteins were digested
115 to peptides and analysed by liquid chromatography tandem mass spectrometry (LC-MS/MS) followed by
116 label-free data dependent acquisition (DDA) quantitation to determine their relative abundance (S1 Table).
117 Identified proteins were used to generate smaller, defined sets of sequences to use in the cross-linking data
118 analysis workflow.

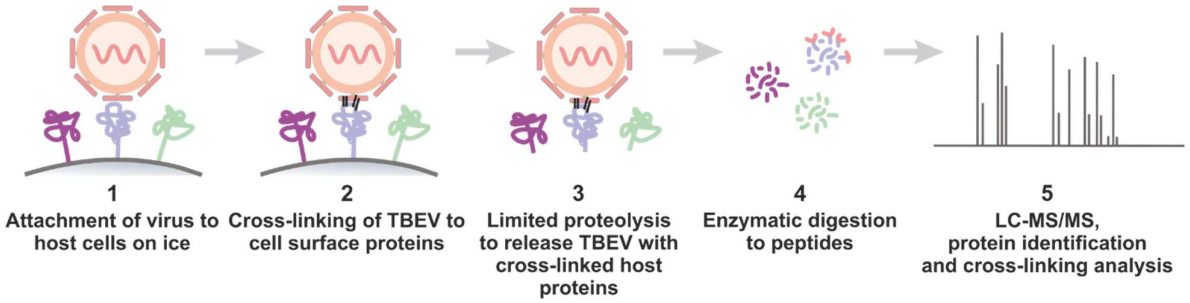

119

120 ***Fig 2: Schematic representation of cross-linking workflow.*** *1. TBEV was allowed to attach to metabolically-*
121 *stalled SK-N-SH cells. 2. TBEV-host PPIs were stabilised by chemical cross-linking with DSS. 3. Cell-surface*
122 *associated proteins, and cross-linked TBEV were released from the cell surface using limited proteolysis. 4.*
123 *The released proteins were digested to peptides. 5. Peptides were analysed by LC-MS/MS and host and viral*
124 *proteins identified and quantified using label-free DDA. Identified host proteins were analysed to identify*
125 *cross-links between the host proteins and TBEV.*

126 For cross-linking, we used four different cross-linker concentrations, in addition to a negative control
127 sample to which no cross-linker was added. Each condition was repeated in triplicate, and the experiment
128 repeated three times independently with different TBEV preparations and cell line passages, yielding 9
129 replicates per cross-linker concentration. The samples were initially analysed by immunoblotting of the
130 TBEV E and C Proteins (Fig 3). The presence of higher molecular weight bands greater than 100 kDa in
131 samples treated with DSS confirms cross-linking (Fig 3). The C protein has been shown to form antiparallel
132 dimers in the crystal and NMR structures of other flaviviruses [29–31]. We identified a band with a

133 molecular weight corresponding to that of C protein dimers, indicating that the C protein dimerizes in TBEV

134 (Fig 3).

135

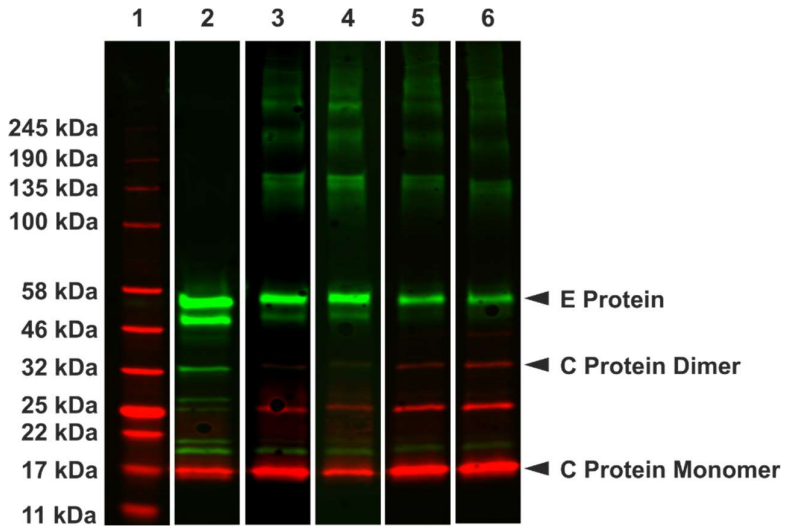

136

137 ***Fig 3: Immunoblot analysis of the TBEV E and C proteins in cross-linked samples.*** *The TBEV C protein in*

138 *shown in red and the TBEV E protein in green. Lane 1- protein marker; Lane 2- negative control with 0 mM*

139 *DSS, Lane 3- cross-linking with 0.1 mM DSS; Lane 4- cross-linking with 0.25 mM DSS; Lane 5- cross-linking*

140 *with 0.5 mM DSS; Lane 6- cross-linking with 1mM DSS. Higher molecular weight bands greater than 100 kDa*

141 *corresponding to the cross-linking of E and C to other proteins can be seen in lanes 2-5. Lower molecular*

142 *weight bands less than 50 kDa corresponding to the partial cleavage of the viral proteins during the limited*

143 *proteolysis step are also observed in all lanes.*

144 Identification of cross-linked peptides is computationally challenging as all primary amine-primary amine

145 combinations in a given sequence database need to be considered. To reduce the search space for cross-

146 linked peptide identification, proteins identified by DDA were probed for cross-links in batches (see

147 materials and methods). A total of 7167 spectral observations of cross-linked peptides were identified using

148 pLink2 at a false discovery rate (FDR) of 5%, excluding interfaces supported by cross-linked peptides

149 identified in the negative controls, which correspond to false positives likely arising from erroneous peptide

150 matches in the complex proteome background (S2 Table) [28]. Spectral observations of cross-links between

151 two peptides within the same protein (intraprotein PPIs) accounted for the majority of the observations
152 (5589), compared to 1578 for those identified between two peptides from different proteins (interprotein
153 PPIs). Intraprotein cross-links have been consistently shown to make up a higher proportion of spectral
154 observations within cross-linked datasets, as two residues within the same protein are highly likely to be in
155 close physical proximity within the cell, leading to an increased cross-linking frequency [32,33]. In total,
156 1697 different cross-linked interfaces were observed, and on average each interface was supported by 4.2
157 spectral observations. The cross-linked interfaces map to a network of 698 PPIs, consisting of 588 host
158 proteins and the 3 viral structural proteins. Overall, 66.3 % of the unique PPIs were attributed to
159 interactions between host proteins, 33.5 % to virus-host interactions and only 0.2 % to intraviral
160 interactions. We also identified intraprotein cross-links in 297 host proteins and the TBEV C and E proteins.

161 The confidence of the cross-linking dataset can be investigated by examining the spatial distances between
162 cross-linked residues for protein complexes where high-resolution structures or reliable homology models
163 are available. As intraviral protein interactions account for 62 % of the detected spectral observations, we
164 used the intraviral cross-links as an internal control to assess the confidence level for the dataset.

165 Mapping of intraviral cross-links

166 The published mature TBEV structure and homology models of the immature virus and C protein dimer
167 were used to accurately measure cross-link distances. The C-score of the homology models were -0.65 (C
168 protein), 2.00 (E protein) and 0.57 (prM protein) [34–36] . We measured the distance between cross-linked
169 residues and applied a maximum distance constraint of 30 Å between the lysine or N-terminus Cα (Table 1
170 and Figs 1 and 4) [37]. In total, 24 cross-links were mapped onto the viral structural proteins, and 22 fell
171 within the accepted distance range. Overall, 14 of the cross-links satisfied the distance constraint in both
172 the mature and immature TBEV structures, six were only acceptable in the mature structure and two in the
173 immature structure. Cross-links with acceptable distances in only the mature structure were identified by
174 2089 spectral observations compared to 31 for those only accepted in the immature structure,
175 demonstrating that the majority of the virus particles in the analysed samples were mature.

176 **Table 1: Intraviral cross-links identified, the corresponding average expectation value and SVM score of**

177 **the peptide spectrum matches, and distances in the mature and immature virus structures**

Cross-link Type	Protein 1	Protein 2	Residue 1*	Residue 2*	Mean E-Value	Mean SVM Score	Number of Spectral observations	Distance Between Cα Carbons Virion	Distance Between Cα Carbons Immature Virus
Intradimer/ Intertrimer	E Protein	E Protein	251	284	0.59	0.07	1346	16.74	47.74^
Intramonomer	E Protein	E Protein	64	126	0.25	0.08	939	12.10	11.95
Intramonomer	E Protein	E Protein	300	161	0.02	0.02	910	17.42	15.99
Intramonomer	E Protein	E Protein	118	69	0.13	0.11	315	9.47	9.08
Interdimer/ Intertrimer	E Protein	E Protein	136	309	0.48	0.10	265	17.25	32.41^
Interdimer/Intertrimer	E Protein	E Protein	309	69	0.09	0.10	172	17.88	30.87^
Intradimer	E Protein	M Protein	266	1	0.42	0.15	155	8.79	N/A
Interdimer/ Intertrimer	E Protein	E Protein	118	309	0.34	0.06	150	18.54	30.67^
Intramonomer/ Intradimer	C Protein	C Protein	10	25	0.41	0.06	63	23.18/23.68	23.18/23.68
Intramonomer	E Protein	E Protein	64	69	0.35	0.16	34	15.26	14.58
Interdimer/ Intertrimer	E Protein	E Protein	251	311	1.00	0.03	23	31.63^	28.63
Intramonomer/ Intradimer	C Protein	C Protein	20	10	0.09	0.02	19	16.45/24.22	16.45/24.22
Intramonomer/ Intradimer	C Protein	C Protein	20	8	1.00	0.35	12	19.30/28.73	19.30/28.73
Interdimer/Intertrimer	E Protein	E Protein	251	309	1.00	0.03	10	26.00	29.38
Intramonomer	E Protein	E Protein	251	69	1.00	0.03	9	9.11	8.26
Interdimer/ Intertrimer	E Protein	E Protein	64	161	1.00	0.06	8	39.39^	30.06
Interdimer/Intertrimer	E Protein	E Protein	64	309	1.00	0.30	4	25.91	27.17
Intramonomer	E Protein	E Protein	309	407	1.00	0.41	3	41.09^	43.78^
Intramonomer	C Protein	C Protein	20	25	0.69	0.22	3	7.12/32.63^	7.12/32.63^
Intramonomer	E Protein	E Protein	309	408	1.00	0.50	2	39.54^	41.45^
Intramonomer	E Protein	E Protein	69	124	1.00	0.62	1	26.85	25.98
Intramonomer	E Protein	E Protein	298	309	1.00	0.23	1	25.96	26.46
Intramonomer	E Protein	E Protein	311	309	1.00	0.22	1	6.04	5.60
Interdimer	M Protein	M Protein	1	1	1.00	0.70	1	19.70	N/A

178 *The TBEV polyprotein sequence was obtained from GenBank (accession: AWC08512.1). The C protein corresponds to

179 residues 1-96; the M protein 206-280 and the E protein 281-776. Residue numbers in the table begin from 1 at the

180 start of each protein.

181 ^Distances between cross-linked residues that are greater than 30 Å and are not considered feasible.

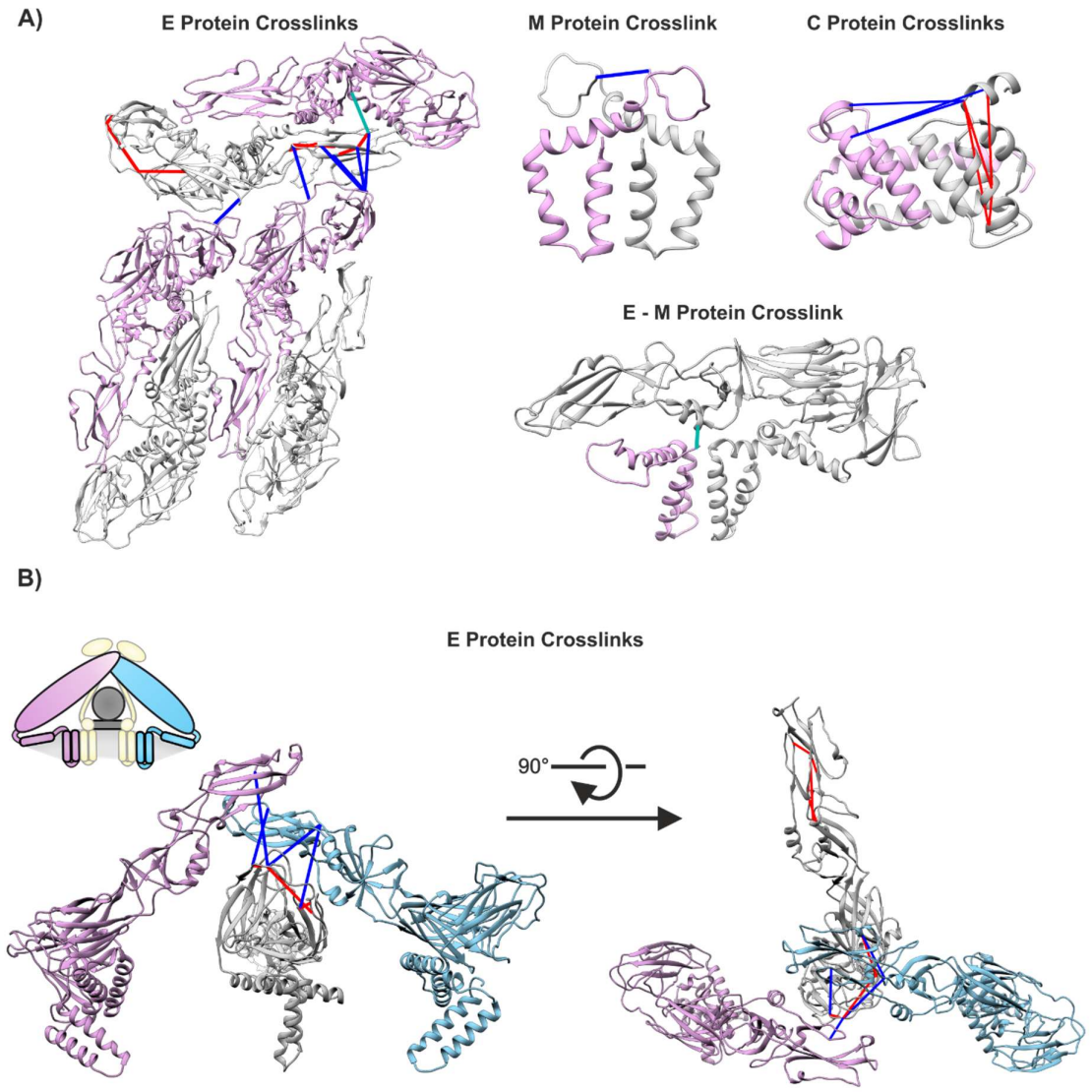

182

183 ***Fig 4: Mapping of intraviral crosslinks.*** *Identified intraviral cross-links with the distances ≤ 30 Å mapped to*

184 *the viral structural proteins are shown above in red, blue and teal. Red cross-links corresponding to*

185 *intramonomer cross-links, teal intradimer cross-links, and blue interdimer or intertrimer cross-links. A)*

186 *Cross-links mapped to the known cryoEM structure of the TBEV virion or the C protein homology model. B)*

187 *Cross-links mapped to the generated homology model of the immature virus, E proteins in trimer 1 are*

188 *coloured in plum and light blue and the E protein in trimer 2 is coloured grey. The schematic diagram*

189 *additionally shows the position of the lipid bilayer (light grey) and the prM protein (light yellow).*

190 Locating the cross-links on the virus structures with distance constraints applied, allowed us to distinguish

191 between three different types of E-E cross-links in the mature virion: intramonomer, intradimer and

192 interdimer cross-links, and two in the immature virus: intramonomer and intertrimer cross-links. As
193 expected, intramonomer E cross-links show similar distances in the mature and immature structures and
194 accordingly the distance constraints are satisfied equally well for both. In contrast, as the E proteins
195 rearrange from trimers to dimers upon virus maturation, only 2 cross-links satisfy the distance constraint in
196 both the intertrimer positions found in the immature virus and the intradimer or interdimer positions
197 found in the mature virus. Two types of cross-links are possible within the C protein dimer, intramonomer
198 and intradimer. In our dataset, three of the four identified C protein cross-links satisfy the distance
199 constraints for both interaction types, making it impossible for us to distinguish between these two
200 alternatives.

201 Two of the intramonomer cross-links between E protein residues 309 and 407 or 408 demonstrate cross-
202 linking lengths of ca. 40 Å in both the mature and immature structures. The cross-links were identified by a
203 low number of spectral observations, 3 for 309-407 and 2 for 309-408, and may arise from interactions
204 between disrupted virions, free E proteins, alternative viral conformations or be false positives. To
205 distinguish between these alternatives, we examined the cross-linked spectra in detail (Fig 5). Fig 5A shows
206 representative spectra for cross-links that satisfy the distance constraint and are identified by a high
207 number of spectral observations, and Fig 5B and C show representative spectra for the two questioned
208 crosslinks. As compared to the spectra shown in Fig 5A, spectra in Fig 5B and C show both a low signal-to-
209 noise ratio and a low sequence coverage for the peptide fragments, and most likely represent false positive
210 hits from background noise.

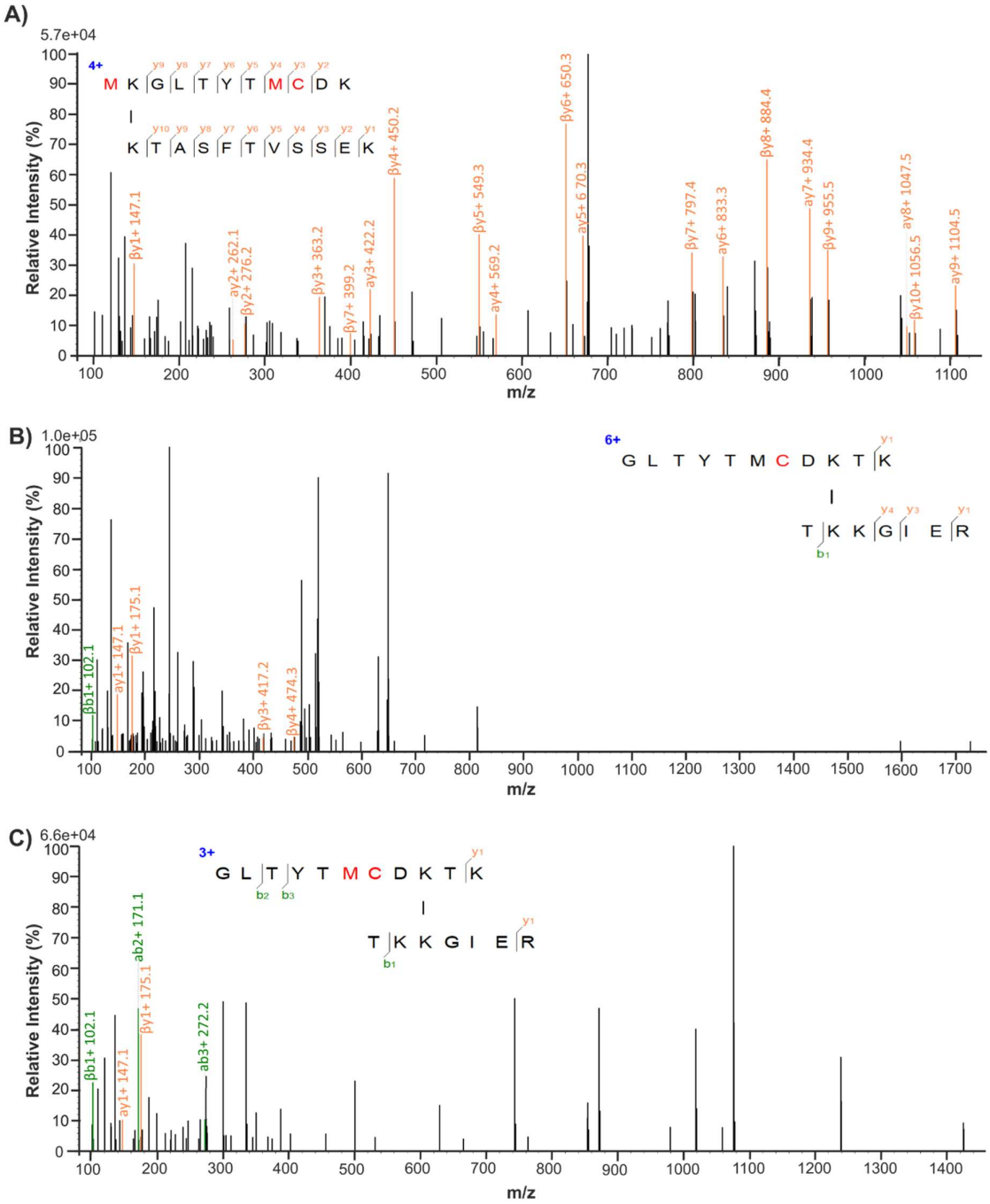

Fig 5: Representative spectra of E protein cross-links that satisfy the distance constraint (< 30 Å) and cross-links with distances > 30 Å. *The cross-linked peptides are shown with the longer α peptide positioned above the shorter β peptide and a connecting line between the cross-linked residues. Modified residues in the peptides are shown in red and the detected beta and gamma fragments shown in green and orange respectively. Peaks corresponding to the detected fragments are coloured and labelled accordingly. The*

charge state of the cross-linked peptide is shown in blue. A) Representative spectrum of E protein cross-link 300-161 that are less than 30 Å and show a high number of spectral observations. B) Representative spectrum for the cross-link 309-407, that has a cross-linking distance of 41.09 Å in the mature structure and 43.78 Å in the immature structure. C) Representative spectrum for the cross-link 309-408 that has a cross-linking distance of 39.54 Å in the mature structure and 41.45 in the immature structure. Cross-links with distances > 30 Å show poor fragmentation and signal to noise ratio in the cross-linked spectral (B and C), compared to cross-links with distances < 30 Å (A).

Based on the imposed distance constraints, we calculated that 91.7 % of the intraviral cross-linked interfaces are identified with high confidence, at a distance threshold of <30 Å indicating that our approach allows detection of specific intra- and inter-protein cross-links with high confidence.

Filtering the cross-linking dataset

The program pLink2 provides two parameters for assessing the confidence of cross-linked peptide spectrum matches (PSM), the expectation value (E-value) and the SVM score [28]. Both the E-value and SVM score describe the probability of a cross-linked PSM being a random match, and have values ranging from 1 to 0, where the smaller the value the more confident the PSM. The SVM score is calculated for every PSM, acting as the prime measure for FDR estimation, whereas the E-value is only calculated for PSMs that pass the FDR threshold [28]. In addition, cross-links may occur due to the sporadic proximity of proteins in the sample, or due to specific cross-linking of interacting proteins. Cross-links identified by more spectral observations have a higher probability of reflecting specific interactions. Therefore, the number of spectral observations per cross-linked interface can provide information about the cross-linking confidence on the protein-protein interaction level. Previous studies have used the E-value, SVM score, number of spectral observations or a combination of the aforementioned to assess the confidence of the identified cross-links but no standardized values have been established [28,38,39]. Here, we investigated the correlation between the E-value, SVM score, number of spectral observations and the acceptable distance constraint (<30 Å) as measured for our intraviral cross-links, to determine confidence parameters for the dataset.

Our data show a correlation between the measured distance of each unique intraviral cross-link and the calculated SVM scores, but not the E-values (Fig. 6, S1 Fig). Consequently, the E-value was not considered as a suitable measure of confidence for this dataset. We observed that intraviral cross-links with distances > 30 Å in both the mature and immature structures (indicated as red bars in Fig. 6) had the 3rd and 4th highest mean SVM scores of the intraviral cross-links (Table 1). Furthermore, cross-links with higher mean SVM scores were only identified by one spectral observation (Table 1). Based on the SVM scores of intraviral cross-links with distances > 30 Å in both the mature and immature structures, we imposed a SVM score threshold of < 0.355, hence discarding 884 of the identified cross-linked interfaces. Interestingly, 97.8 % of the excluded interfaces were identified by only one spectral observation.

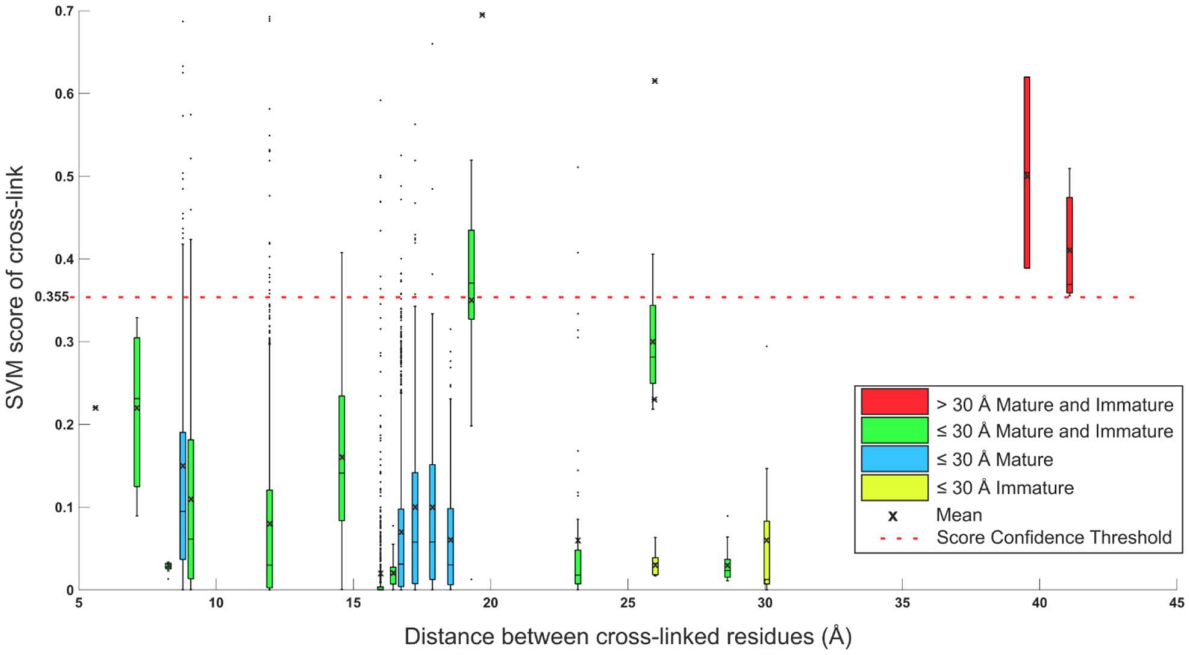

Fig 6: Box and whisker plot of the SVM scores for the intraviral cross-links, plotted against the distance between the cross-linked residues for each cross-link. *The bars are coloured based on whether the distance constraint is satisfied for both the mature and immature conformations (green), only the mature conformation (blue), only the immature conformation (yellow) or not satisfied in either the mature or immature conformation (red). The mean SMV score is marked with a cross. A SVM score confidence threshold of < 0.355 is shown by a red dashed line.*

258 The number of cross-linked spectral observations for 101 randomly selected proteins in the dataset was
259 compared to the average spectral count of these proteins across all the samples in the DDA analyses (S1
260 File). The number of spectral observations for cross-linked peptide pairs for these same 101 selected
261 proteins was also compared to the number of lysine residues present within each protein (S1 File). No
262 correlation was observed in either of these cases; so, neither protein abundancy nor lysine content affect
263 the data content (S1 File). Therefore, the number of spectral observations was used in a non-biased
264 manner to assess the confidence of each unique cross-link to reduce the dataset for analysis further.

265 Here, we filtered the data in a stepwise manner, first on the PSM level using the SVM score and secondly
266 on the protein-protein interaction level using the number of spectral observations. A cross-linked interface
267 was considered to be of high confidence if it had an SVM score < 0.355 and was identified by ≥ 2 spectral
268 observations. Filtering the data in the reverse order would lead to inclusion of interactions only supported
269 by one high confidence spectral observation. The filtered cross-linking dataset consisted of 218 cross-linked
270 interfaces, 36.7 % of which were attributed to virus-host PPIs (S3 Table).

271 Virus-host protein-protein interactions

272 Virus-host PPIs were identified between TBEV and 61 host proteins in the filtered cross-linking dataset. In
273 total, 59 proteins were shown to interact with the TBEV E protein and 2 with the M protein. Cross-links with
274 the M protein form between N-terminal serine of mature M and the host proteins. As the M protein is
275 buried and not accessible for cross-linking in the mature virion, these interactions likely occur between the
276 host proteins and disrupted virions, free M protein, or conformations that have yet to be described.

277 E -host PPIs were mapped to eight different lysine residues on the outer surface of the virion (E protein
278 residues 118, 126, 136, 161, 251, 280, 300, and 336; Fig 5), indicating that the host proteins were indeed
279 interacting with assemble capsids. Only six of these residues shown in blue are also accessible on the outer
280 surface of the immature particle, as residue 336 is obscured by other E proteins and residue 251 by prM
281 (Fig 7). The cross-linked lysine residues are distributed evenly across the surface of the E protein, showing
282 no preference for domains I, II or III (Fig 7).

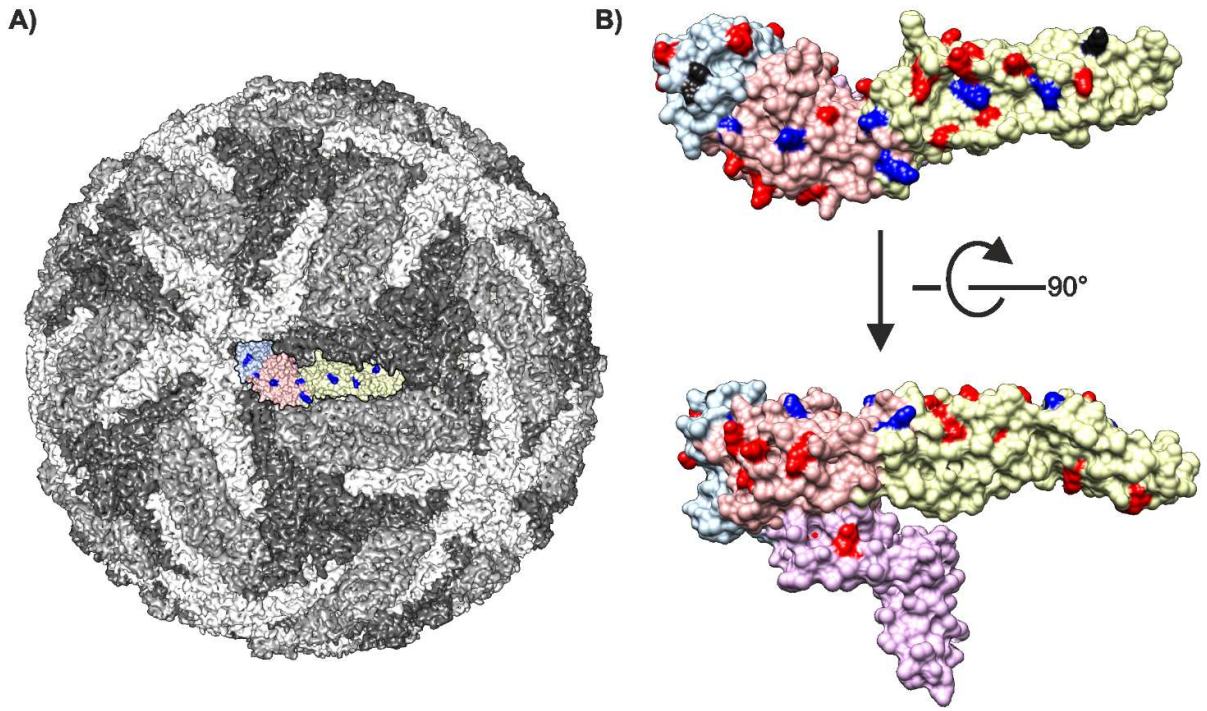

283

284 ***Fig 7: Visualisation of E protein lysine residues that form cross-links with host proteins.*** *A) Surface*
285 *representation of the TBEV virion (PDB accession: 5O6A) [24]. The three E proteins within each asymmetric*
286 *unit are shown in white, grey and dark grey. One E protein monomer is shown in colour (TBEV domain I is*
287 *shown in peach, domain II in yellow, domain III in lilac with the cross-linked lysines shown in blue. B)*
288 *Mapping of the cross-linked lysines on the structure of the E protein (PDB accession 5O6A). Lysines detected*
289 *with cross-links are shown in blue if located on the surface of both the mature and immature virus and black*
290 *for those only located on the surface of the mature virus; lysines without cross-links are shown in red. TBEV*
291 *domain I is shown in peach, domain II in yellow, domain III in light blue and domain IV in lilac.*

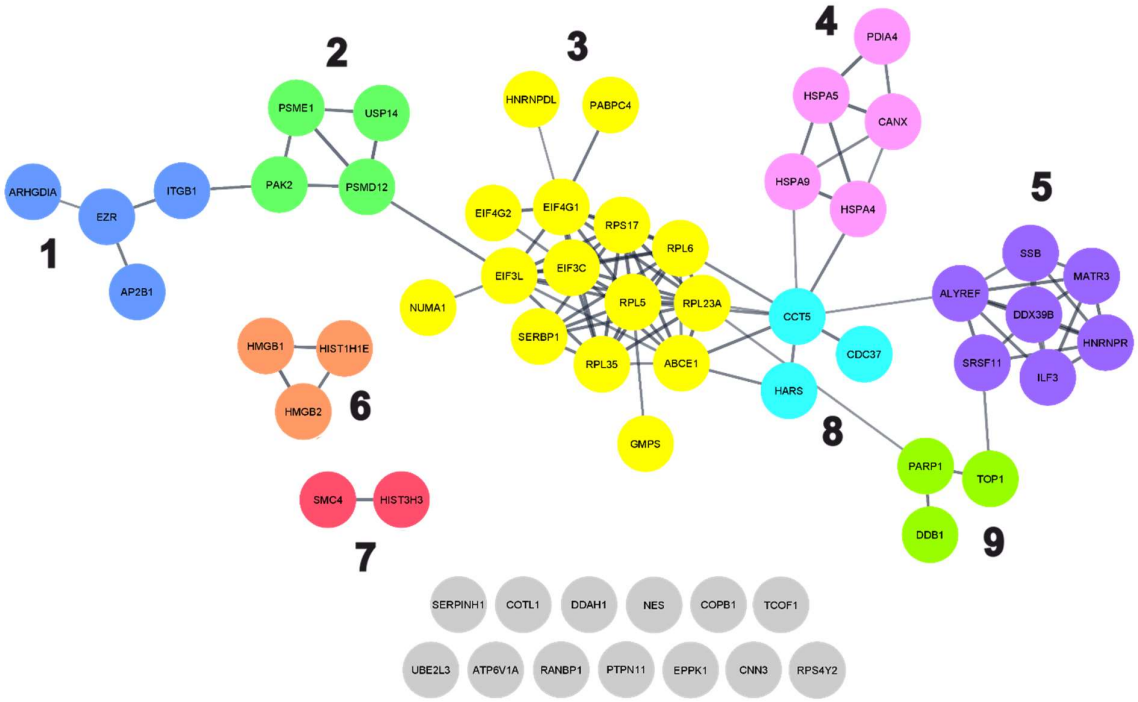

Fig 8: String network of 59 host proteins identified as interacting with the TBEV E protein in the filtered cross-linking dataset. *The string-database network shows both direct and indirect protein interactions and is clustered based on the combined score associated with each interaction, using the Markov clustering algorithm [40]. Proteins are coloured based on the clustering and each cluster is numbered (1-9). Proteins that do not have any known interactions with other host proteins identified in the filtered cross-linking dataset are shown in grey.*

We performed String-database analysis to identify if any of the 59 E protein-interacting host proteins also interact with each other (Fig 6) [40]. In total, 46 proteins were shown to interact with at least one other protein, and nine interaction clusters were identified. This suggests that TBEV may interact with both individual proteins and larger protein complexes. Gene ontology (GO) analysis (S4 Table) of the clusters indicates that proteins in clusters 1, 2 and 4 are located in the extracellular region (GO:0005576), at the plasma membrane (GO:0005886) or in extracellular exosomes (GO:0070062). Clusters 1 and 2 show enrichment for receptor-mediated biological processes, including receptor-mediated endocytosis (GO:0006898; cluster 1), and receptor-mediated signalling (GO:0038095, GO:0050852, GO:0002223; cluster

307 2), whereas proteins in cluster 4 are involved in protein transport (GO:0015031). Cluster 3 is the largest
308 cluster and consists of proteins found in the cytosol (GO:0005829) predominantly as part of ribosomes
309 (GO:0005840), ribonucleoprotein complexes (GO:1990904) or the eukaryotic translation initiation factor 4F
310 complex (GO:0016281). Other cytosolic proteins belong to cluster 8 (GO:0005829) and are involved in
311 protein folding (GO:0006457) or translation (GO:0006412). Finally, proteins in clusters 5, 6, 7 and 9 are
312 primarily found in the nucleus (GO:0005634) and are involved in RNA processing (GO:0006396),
313 posttranscriptional regulation of gene expression (GO:0010608; cluster 5), and chromosome organisation
314 (GO:0051276; clusters 6, 7 and 9). Importantly, many proteins primarily located in the cytosol or nucleus
315 (clusters 3, 5-9) are also found in the plasma membrane or extracellular regions where they perform
316 alternative biological functions; for example, HMGB1 (UniprotKB:P09429; cluster 6), functions as a
317 nonhistone nucleoprotein in the nucleus and an inflammatory cytokine in the extracellular region [41]. In
318 addition, GO analysis identified 19 proteins that are associated with immune system process, and 11
319 proteins associated with the cytoskeleton or cytoskeletal rearrangement.

320 # Discussion

321 In this study, we present a chemical cross-linking proteomics approach to simultaneously identify TBEV-
322 neuroblastoma cell PPIs and their interaction interfaces. We used metabolically-stalled cells to adsorb and
323 cross-link virus only to the cell surface, hoping to primarily enrich proteinaceous cell surface interactions.
324 The cross-linked proteins were released by limited proteolysis. Analysis of this highly complex protein
325 mixture by LC-MS/MS generated a large database of spectra containing four different peptide species with
326 the minority being cross-linked. In addition, cross-linked peptides are the least well-fragmented in the
327 database. In the next step, the pLink2 software compares the database of spectra with all of the possible
328 theoretical cross-linker reaction outcomes. This step is a clear bottle neck in the process as in our hands,
329 only 28 proteins could be analysed at a time, requiring multiple batch runs. Here, we optimised the analysis
330 workflow in order to extract the most significant virus-host PPIs from our complex data. Firstly, we reduced
331 the cross-linking search space by only analysing proteins identified by linear peptides in the samples.

332 Secondly, we have an internal validation control in the sample. We identified high-confidence intraviral
333 crosslinks using both the known and predicted three-dimensional structures of TBEV and the known length
334 of the chemical cross-linker. Then, we correlated the high confidence cross-links with the SVM score and
335 the quality of the spectra, allowing us to use an SVM score cut-off < 0.355 for the entire dataset. Finally, we
336 imposed a spectral count cut-off ≥ 2 to select for the most specific protein interactions. Using this method,
337 we identified 22 high confidence unique intraviral cross-links and 59 high confidence unique virus-host PPIs
338 between the surface of TBEV and human neuroblastoma cells. These proteins form a robust and reliable
339 dataset that can be investigated further for their roles in the virus life cycle. They could be targets for
340 intervention.

341 Our approach presents four major advantages over alternative approaches used to identify virus-host PPIs
342 described in the literature: 1) The wild-type virus interacts with cellular proteins on the surface of
343 neuroblastoma cells. In comparison, affinity purification, yeast two hybrid and protein microarrays detect
344 interactions in artificial systems [8–12]. Therefore, the expression levels, presentation and glycosylation
345 state of the host and viral proteins may differ from that in natural infections, leading to both false positives
346 and false negatives; 2) When fully assembled viral particles are used as bait, the capsid proteins are in the
347 right biological conformation and molecular context for infection. In contrast, single recombinant bait
348 proteins used in affinity purification, yeast two hybrid, protein microarrays and BioID may not be [8–12,16].
349 For instance, the monomeric Dengue virus ancillary receptor, DC-SIGN binds across two neighbouring E
350 proteins on the capsid [42]. In our virus-based protocol, there would be 90 such sites for the DC-SIGN
351 interaction giving both the correct biological context, but also increasing the avidity of the interactions; 3)
352 The virus interacts with cellular proteins prior to crosslinking. In contrast, in the previously described
353 approaches using trifunctional cross-linkers or BioID, the viral proteins are first conjugated to the cross-
354 linker or biotin ligase prior to the interaction with cells. Conjugation may require genetic modification [13–
355 17]. Consequently, interactions may be missed if the modification sterically hinders the binding region.
356 Here we could identify PPIs, under near-physiological conditions, without the need for genetic
357 manipulation; 4) The clearest advantage in our approach is that we map virus-host PPIs directly from the

358 cross-linked peptides. This gives us additionally information about which residues are within 30 Å of each
359 other and form the interaction interface.

360 Although this approach shows promise for detecting a wide-range of virus-host PPIs, there are also some
361 challenges. The complete coverage of the interaction space is limited by the accessibility of surface cross-
362 linkable lysine residues and the sample complexity. In order to detect an interaction, there must be cross-
363 linkable residues on both sides of the interaction interface within 30 Å of each other. Furthermore, in
364 complex systems containing a higher number of protein species, the number of cross-links per species is
365 lower in comparison to simpler systems. Consequently, interactions that occur in lysine deficient regions or
366 with low frequency cannot be detected, leading to an incomplete picture of the interaction interface or
367 failure to detect the PPI. Performing parallel experiments using chemical cross-linkers with different lengths
368 or reactive residues such as arginine, aspartate or glutamate, could overcome this limitation [43,44]. Simple
369 cross-linking experiments including only the virus and a single interaction partner can be used to ensure
370 complete coverage of the 3D interaction space once interesting PPI have been identified.

371 Having considered the potential advantages and challenges of this protocol, we will now consider potential
372 biological implications. Laminin binding protein has previously been suggested as a TBEV receptor. It was
373 present in our dataset, but no cross-links were identified to TBEV [45,46]. Our data do not support that
374 laminin binding protein is a TBEV receptor in this cell line. However, we have identified proteins that are
375 associated with the early stages of viral infection in other viruses, including ITGB1, ATP6V1A, EZR, HSPA9,
376 and HSPA5. ITGB1 as an entry receptor for a large number of viruses including, cytomegalovirus, Epstein-
377 Barr virus, human parvovirus B19, and mammalian reovirus [47–50]. ATP6V1A directly interacts with rabies
378 viral matrix protein facilitating uncoating [51]. EZR is an essential host factor required for the entry of
379 Japanese encephalitis virus into human brain microvascular endothelial cells [52]. HSPA9 has been
380 identified as a putative receptor for Tembusu virus [53].

381 HSPA5 (Cluster 4, Fig 6) has been identified as a receptor for several flaviviruses including, Zika and
382 Japanese encephalitis where HSPA5 was shown to affinity purify with recombinant E protein domain III, but

383 the interaction context in virions has not been studied [55,56]. HSPA5 is a multifunctional regulator of
384 endoplasmic reticulum homeostasis, playing an important role in protein processing and quality control
385 [58–61]. It is located both in the endoplasmic reticulum lumen and on the outer surface of the plasma
386 membrane in many cell types including neurons [62–65]. HSPA5 consists of 2 domains, a nucleotide-binding
387 domain that binds ATP, and a substrate-binding domain that binds and stabilises partially folded or folded
388 proteins [66]. Here we identified four spectral observations mapping to the TBEV E hinge region (residue
389 136) and the HSPA5 substrate binding domain residues 521 and 516 (Fig 9). Therefore, the interaction
390 between HSPA5 and the E protein hinge region could constitute a unique binding interface, or be part of a
391 larger interface that also binds domain III consistent with other flavivirus studies [53–55,57]. We
392 hypothesize that HSPA5 could interact with both the hinge region of one E monomer and domain III of an
393 adjacent E monomer at the 3-fold axis, where the regions are in close spatial proximity (Fig 9).
394 Interestingly, Fab fragments of the TBEV neutralising antibody 19/1786 have been shown to bind across
395 this interface at the 3-fold axis potentially preventing the HSPA5 interaction[24]. Although, no cross-links
396 were detected between domain III and HSPA5 in our study, this can be partly explained by poor lysine
397 availability. Structural bioinformatics studies of the Zika virus domain III-HSPA5 interaction do not detect
398 any interacting lysine residues on HSPA5[67].

399

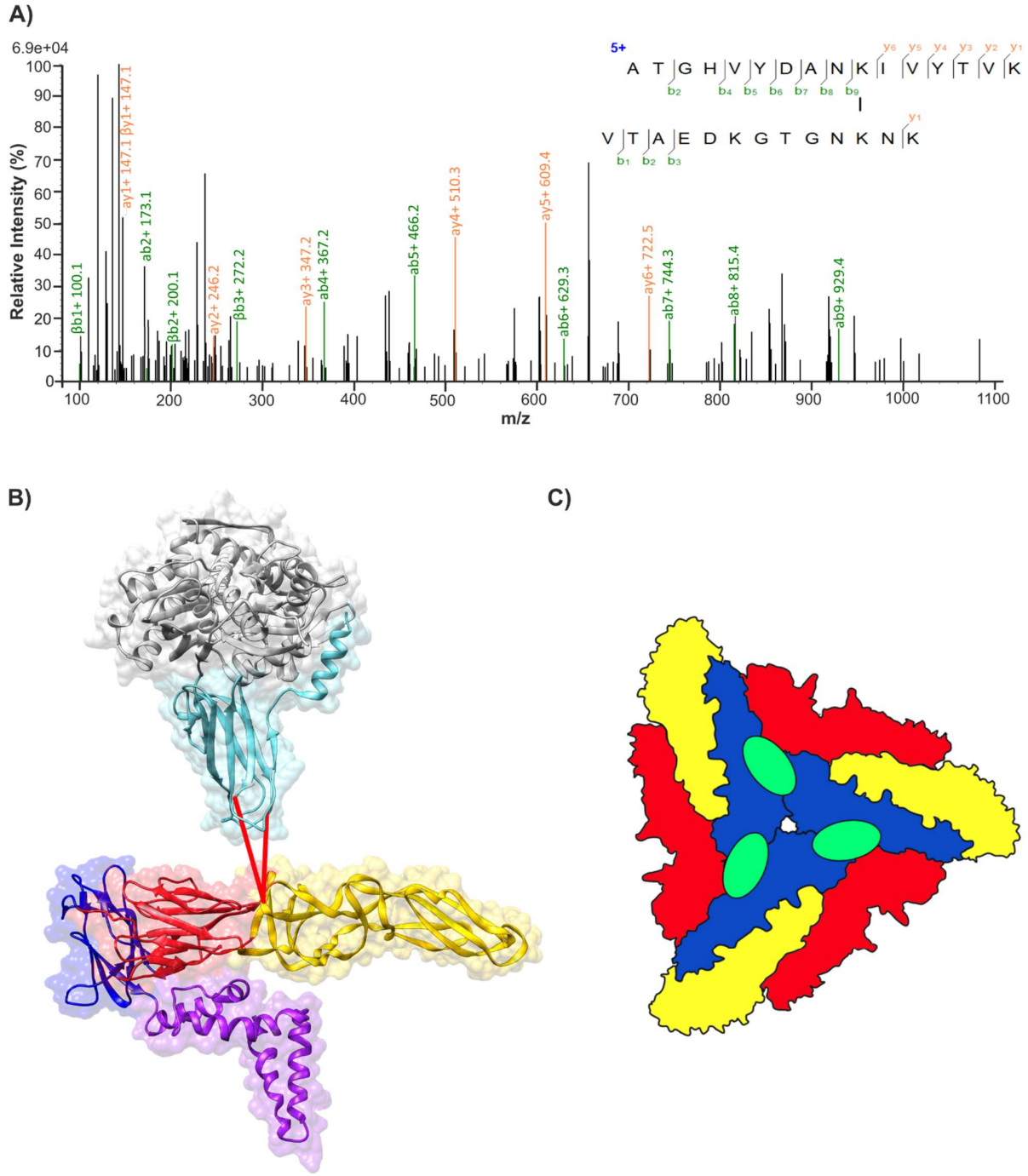

Fig 9: Cross-linking of HSPA5 and TBEV E protein *A) Assigned spectrum for the peptide associated with the HSPA5-E protein interaction. B) TBEV E protein (PDB accession 5O6A) and HSPA5 (PBD accession 6ZMD) were placed in close proximity to allow for the visualisation of the cross-links, indicated here with red lines. TBEV E protein domain I is shown in red, domain III in dark blue, domain II in yellow and domain 4 in purple. HSPA5 substrate-binding domain is shown in light blue and the remainder of the protein in grey. C)*

406 *Schematic representation of speculated HSPA5 binding region on the mature virus. The three E proteins*
407 *within each asymmetric unit are shown in blue, red, and yellow. The proposed HSPA5 binding site is shown*
408 *in green*.

409 After the virus has attached to the cell surface, the next step is to enter the cells either through clathrin-
410 mediated endocytosis or macropinocytosis, and we found evidence for both pathways being used. We
411 identified AP2B1 in the GO analysis that binds to the clathrin heavy chain [68]. We also identified an
412 abundance of cytoskeletal proteins and cytoskeletal remodelling proteins required in macropinocytosis
413 including, NES, NUMA1, ITGB1, EZR, PAK2, COTL1, CCT5, CNN3, EPPK1 and RANBP1. This supports the
414 hypothesis that macropinocytosis is used by TBEV as well as Dengue virus [69].

415 Conclusions

416 In this study, we present a XL-MS method to identify and map transient virus-host PPIs under near-
417 physiological conditions, without the need for genetic modification. Using this method, we identified 59
418 high confidence virus-host PPIs between TBEV and the surface of neuroblastoma cells. These proteins form
419 a robust and reliable dataset that can be investigated further for functional relevance in targeted follow-up
420 experiments. The presented methodologies are generally applicable to other virus-host systems and can
421 assist in expanding our knowledge of viral infections.

422 Materials and methods

423 Viruses and cells

424 Neuroblastoma SK-N-SH cells (ECACC 86012802) were maintained in Dulbecco's modified Eagle's medium
425 (DMEM) (Sigma) supplemented with 10 % heat inactivated FBS (Gibco), 100 µg/ml of penicillin-
426 streptomycin mix (PenStrep) (Sigma) and 2 mM L-glutamine (Sigma), at 37 °C and under a 5 % CO_2
427 atmosphere. For virus propagation, cells were infected with TBEV strain, MG569938 Kuutsalo-14 *Ixodes*
428 *ricinus* Finland-2017, at a MOI of 0.003, in Dulbecco's modified Eagle's medium (DMEM) (Sigma)

429 supplemented with 2 % heat inactivated FBS (Gibco), 100 µg/ml of penicillin-streptomycin mix (PenStrep)
430 (Sigma), 2 mM L-glutamine (Sigma) and 0.35 µM rapamycin and incubated at 37 °C for 3 days under a 5 %
431 CO_2 atmosphere. Virus-containing supernatant was aspirated and centrifuged at 4500 x g for 5 minutes to
432 remove cell debris. Cleared supernatant was aliquoted into cryopreservation vials and frozen at -80 °C. Viral
433 titers were determined using plaque-forming assay. SK-N-SH cells were grown on a 6-well plate, infected
434 with ten-fold serial dilutions of the virus and incubated for 1 hour at 37 °C, under a 5 % CO_2 atmosphere.
435 Overlay medium (Minimum Essential Medium Eagle, PenStrep and 2 mM L-glutamine, 1.2 % avicel) was
436 added to each well and the cells incubated for 4 days at 37 °C, under a 5 % CO_2 atmosphere. After 4 days
437 the cells were fixed with 10 % formaldehyde, stained with crystal violet and the plaques counted to
438 determine the number of plaque forming units per ml (PFU/ml).

439 Production of amino acid free virus stock

440 SK-N-SH cells were grown to 90% confluence, washed twice with PBS and the medium changed to amino
441 acid free DMEM (Genaxxon) supplemented with 100 µg/ml of penicillin-streptomycin mix (PenStrep)
442 (Sigma) and rapamycin 0.35 µM (selleckchem). Cells were infected with TBEV, at multiplicity of infection 1,
443 and incubated at 37 °C for 4 Days, under a 5 % CO_2 atmosphere. Virus-containing supernatant was
444 aspirated and centrifuged at 4500 x g for 5 minutes to remove cell debris. The virus was pelleted through a
445 30 % sucrose cushion in HNE buffer (20 mM HEPES pH 8.5, 150 mM NaCl, 1 mM EDTA), 2 h, 27000 rpm, 4
446 °C. The virus pellet was then resuspended in amino acid free DMEM (Genaxxon) overnight, 4 °C, with mild
447 shaking. The virus was aliquoted into cryopreservation vials and frozen at -80 °C. The stock was titered as
448 described above. The typical obtained titer was 5 x 10^9 pfu/ml.

449 Cross-linking of TBEV with SK-N-SH cells

450 SK-N-SH cells were grown in a 6 well plate to 90 % confluence, washed twice with PBS, and the medium
451 changed to amino acid free DMEM (Genaxxon) supplemented with 100 µg/ml of penicillin-streptomycin
452 mix (PenStrep) (Sigma). The cells were incubated overnight at 37 °C, under a 5 % CO_2 atmosphere. The cells
453 were infected with TBEV at a MOI of 375 for 60 min, with rocking, on ice. Heavy/light disuccinimidyl

454 suberate cross-linker (DSS-H12/D12, Creative Molecules Inc., www. creativemolecules.com) resuspended in
455 dimethylformamide (DMF) was added to final concentrations of 0, 100, 250, 500 and 1000 µM and
456 incubated for 60 min, with rocking on ice. The cross-linking reaction was quenched with a final
457 concentration of 50 mM ammonium bicarbonate with rocking, on ice. The SK-N-SH cell surface proteins
458 with attached TBEV virions were digested off with 1.25 µg trypsin (Promega) and the supernatant collected.
459 Finally, cell debris was removed via centrifugation (16,000 x g, 5 min), the supernatant recovered, and the
460 samples prepared for mass spectrometry (Fig 2).

461 Immunoblot analysis

462 Proteins were resolved in 4-20 % SDS-PAGE, transferred onto a nitrocellulose membrane, and probed using
463 anti-Langat E protein (BEI NR-40318; 1:1000 dilution) and C protein (57) (1:1000 dilution) antibodies in 5 %
464 milk, tris-buffered saline 0.1 % tween-20 (TBST) [70]. The protein bands were visualised using IR800 and
465 IR680-conjugated secondary anti-rabbit (Li-COR, 926-68071) and anti-mouse antibodies (KPL, 072071806)
466 diluted 1:10,000 in tris-buffered saline 0.1 % tween-20 (TBST). The membrane was imaged using the
467 Odyssey infrared imaging system (Li-COR).

468 Preparation of cross-linked samples for mass spectrometry

469 Samples from cross-linking were first denatured with 8 M urea-100 mM ammonium bicarbonate. The
470 cysteine bonds were then reduced with 5 mM tris(2-carboxyethyl) phosphine (37 °C, 60 min, 400 rpm) and
471 alkylated with 10 mM 2-iodoacetamide (22 °C, 30 min, in the dark). Protein digestion was then performed
472 with 0.1 µg/µl sequencing-grade lysyl endopeptidase (Wako chemicals) (37 °C, 2h, 400 rpm). Following the
473 dilution of the sample with 100 mM ammonium bicarbonate to a final urea concentration of 800 mM the
474 proteins were digested further with 0.2 µg/µl trypsin (Promega) (37 °C, 18h, 400 rpm). Digested samples
475 were then acidified with 10% formic acid to a pH of 3.0, and the peptides were subsequently purified with
476 C18 reverse-phase spin columns according to the manufactures protocol (Microspin Column, SS18V, The
477 Nest Group, Inc). Peptides were then dried in a speedvac and reconstituted in 2% acetonitrile, 0.2% formic
478 acid prior to mass spectrometric analyses

479 ## Liquid chromatography tandem mass spectrometry

480 All peptide analyses were performed on a Q Exactive HFX mass spectrometer (Thermo Scientific) connected
481 to an EASY-nLC 1200 ultra-high-performance liquid chromatography system (Thermo Scientific). The
482 peptides were loaded onto an Acclaim PepMap 100 (ID 75µm x 2 cm, 3 µm, 100 Å) pre-column and
483 separated on an EASY-Spray column (Thermo Scientific; ID 75 µm × 25 cm, column temperature 45 °C)
484 operated at a constant pressure of 800 bar. A linear gradient from 4% to 45% of 0.1% formic acid in 80%
485 acetonitrile was run for 50 min at a flow rate of 300 nl/min One full MS scan (resolution 60,000@200 m/z;
486 mass range 350 to 1600 m/z) was followed by MS/MS scans (resolution 15,000@200 m/z) of the 15 most
487 abundant ion signals. The precursor ions were isolated with 2 m/z isolation width and fragmented using
488 higher-energy collisional-induced dissociation at a normalized collision energy of 30. Charge state screening
489 was enabled, and precursors with an unknown charge state and singly charged ions were excluded. The
490 dynamic exclusion window was set to 15 s and limited to 300 entries. The automatic gain control was set to
491 3×10^6 for MS and 1×10^5 for MS/MS with ion accumulation times of 110 and 60 ms, respectively. The
492 intensity threshold for precursor ion selection was set to 1.7×10^4.

493 ## MS data analysis

494 Raw DDA data was converted to gzipped and Numpressed mzML [71] using MSconvert from the
495 ProteoWizard, v3.0.5930 suite [72]. All data was managed and analysed using openBIS [73]. The acquired
496 spectra were analysed using the search engine X! Tandem (2013.06.15.1-LabKey, Insilicos, ISB) [74], OMSSA
497 (version 2.1.8) [75] and COMET (version 2014.02 rev.2) [76] against an in-house compiled database
498 containing the reviewed *Homo sapiens* reference proteome (UniProt proteome ID UP000005640) and the
499 TBEV proteome (GenBank accession: AWC08512.1), yielding a total of 78121 protein entries and an equal
500 amount of reverse decoy sequences. Full tryptic digestion was used allowing two missed cleavages.
501 Carbamidomethylation (C) was set to static and oxidation (M) to variable modifications, respectively. Mass
502 tolerance for precursor ions was set to 0.2 Da, and for fragment ions to 0.02 Da. Identified peptides were
503 processed and analysed through the Trans-Proteomic Pipeline (TPP v4.7 POLAR VORTEX rev 0, Build

504 201403121010) using PeptideProphet [77]. The false discovery rate (FDR) was estimated with Mayu
505 (v1.7)[78] and peptide spectrum matches (PSMs) were filtered with protein FDR set to 1% resulting in a
506 peptide FDR >1%. Proteins were filtered to remove hits identified by only 1 unique peptide, and an average
507 spectral count of < 2 across all samples. The protein names and corresponding UniProt ID are given in
508 Supplementary information 1.

509 Cross-link identification

510 In total 874 proteins that were identified by 2 or more unique peptides, and an average spectral count of
511 ≥2 across all samples in the DDA data were probed for cross-links. Cross-links between the TBEV structural
512 proteins and host proteins were identified using the pLink2 software package [28]. In order to reduce the
513 search space for cross-link identification the data was analysed in 35 batches. The raw data dependent
514 acquisition data, and compiled FASTA file databases containing a total of 28 protein sequences, from 25
515 different host proteins and the 3 viral structural protein were used as the software input. Host protein
516 sequences were obtained from UniProt. The TBEV polyprotein sequence was obtained from GenBank
517 (accession: AWC08512.1), the C protein corresponds to residues 1-96, the M protein 206-280 and the E
518 protein 281-776. The following search parameters were used in the pLink2 software: Conventional cross-
519 linking (Higher-energy C-trap dissociation (HCD)), precursor mass tolerance of 20 ppm; fragment mass
520 tolerance of 20 ppm; peptide length of 6-60; peptide mass of 350-6000 Da, up to 3 missed cleavage sites;
521 carbamidomethylation (C) was set to static modification; and oxidation (M) to variable modification. The
522 results were then filtered using a filtering tolerance of ±10 ppm and a separate FDR >5% at the peptide
523 spectrum matches level. 7716 cross-linked spectral observations were observed across all samples, 302 of
524 these were observed in the negative control samples. In total, 247 cross-linked spectral observations in the
525 0.1-1mM DSS samples corresponded to cross-linked interfaces also identified in negative control samples
526 and were excluded from further analysis.

527 ## Homology modelling, structure visualization and measuring cross-link
528 distances

529 Homology models for the TBEV C protein, immature conformation of the E protein and the prM protein
530 were generated using the I-TASSER (Iterative Threading ASSEmbly Refinement) server [34–36]. A C-score
531 (confidence score for estimating the quality of predicted models by I-TASSER) is generated for each model
532 and can range from -5 to 2, with a higher value signifies a higher confidence and where a C-score > -1.5 is
533 considered good [34–36]. The C-protein homology model was generated using PDB accession 5OW2, and
534 the immature conformation of the E protein, and the prM protein using PDB accession 7L30 as the
535 template. The TBEV polyprotein sequence was obtained from GenBank (accession: AWC08512.1). The
536 sequence for the C protein was obtained from residues 1-96, the E protein residue 281-776, and the prM
537 residues 113-280 in the polyprotein. Generation of the assembled immature virus homology model, and
538 the C-protein dimer was performed in UCSF Chimera [79]. The homology model for the immature virus was
539 generated by superimposing the models for the immature E protein and prM protein onto the assembled
540 immature Spondweni virus (PDB accession 6ZQW) structure, using the MatchMaker function. The
541 homology model for the C protein dimer was generated by superimposing two models of the C protein
542 onto the Zika C protein dimer (PDB accession 5YGH), using MatchMaker. The atomic models were used to
543 position both intraprotein and interprotein cross-links by choosing the distance between Cα atoms in
544 Chimera [24,25].

545 ## Networking and clustering analysis

546 String data were obtained from string database [40] and imported into Cytoscape 3.4 [80] .The following
547 interaction sources were considered: experiments, databases, co-expression, co-occurrence and gene
548 fusion, and interactions with a minimum interaction score of 0.7 are shown. Clusters were generated using
549 the Markov clustering algorithm and gene ontology annotations for each cluster were obtained using
550 GOnet [81].

551 ## Data Availability Statement

552 The datasets generated during and/or analysed in the current study are available in the repositories with
553 the persistent web links: ftp://massive.ucsd.edu/MSV000088272/ [75].

554 The mass spectrometry data has been deposited to the ProteomeXchange consortium via the MassIVE
555 partner repository https://massive.ucsd.edu/ with the dataset identifier PXD029384 [75].

556 # Acknowledgments

557 We thank Markku Varjosalo and Johan Malmström for helpful discussions. The work was carried out in the
558 Instruct Centre Finland supported by grants to SJB from the Swedish Research Council reference number
559 2018-05851; the Academy of Finland grant number 336471, the Sigrid Juselius Foundation grant number
560 95-7202-38. This project (ViBRANT) has also received funding from the European Union's Horizon 2020
561 Research and Innovation Programme under the Marie Skłodowska-Curie grant agreement number 765042.
562 SVB is a fellow of the Doctoral Programme in Integrative Life Science, University of Helsinki. LIAP is a fellow
563 of the Doctoral Programme in Microbiology and Biotechnology, University of Helsinki. We gratefully
564 acknowledge support from the Swedish National Infrastructure for Biological Mass Spectrometry.

565 # Conflict of interests

566 The authors declare that they have no conflict of interest.

567 # References

568 1. Kumar N, Sharma S, Kumar R, Tripathi BN, Barua S, Ly H, et al. Host-Directed Antiviral Therapy. Clin
569 Microbiol Rev. 2020 May 13;33(3):e00168-19, /cmr/33/3/CMR.00168-19.atom.

570 2. Anasir MI, Zarif F, Poh CL. Antivirals blocking entry of enteroviruses and therapeutic potential. J
571 Biomed Sci. 2021 Dec;28(1):10.

572 3. Plavec Z, Pöhner I, Poso A, Butcher SJ. Virus structure and structure-based antivirals. Curr Opin
573 Virol. 2021 Dec;51:16–24.

574 4. Tahir ul Qamar M, Shokat Z, Muneer I, Ashfaq UA, Javed H, Anwar F, et al. Multiepitope-Based
575 Subunit Vaccine Design and Evaluation against Respiratory Syncytial Virus Using Reverse Vaccinology
576 Approach. Vaccines. 2020 Jun 8;8(2):288.

577 5. Wang N, Shang J, Jiang S, Du L. Subunit Vaccines Against Emerging Pathogenic Human
578 Coronaviruses. Front Microbiol. 2020 Feb 28;11:298.

579 6. Roulin PS, Murer LP, Greber UF. A Single Point Mutation in the Rhinovirus 2B Protein Reduces the
580 Requirement for Phosphatidylinositol 4-Kinase Class III Beta in Viral Replication. Pfeiffer JK, editor. J Virol.
581 2018 Sep 12;92(23):e01462-18, /jvi/92/23/e01462-18.atom.

582 7. Barrass SV, Butcher SJ. Advances in high-throughput methods for the identification of virus
583 receptors. Med Microbiol Immunol (Berl). 2020 Jun;209(3):309–23.

584 8. Mukherjee S, Sengupta N, Chaudhuri A, Akbar I, Singh N, Chakraborty S, et al. PLVAP and GKN3 Are
585 Two Critical Host Cell Receptors Which Facilitate Japanese Encephalitis Virus Entry Into Neurons. Sci Rep.
586 2018 Dec;8(1):11784.

587 9. Shapira SD, Gat-Viks I, Shum BOV, Dricot A, de Grace MM, Wu L, et al. A Physical and Regulatory
588 Map of Host-Influenza Interactions Reveals Pathways in H1N1 Infection. Cell. 2009 Dec;139(7):1255–67.

589 10. Jäger S, Cimermancic P, Gulbahce N, Johnson JR, McGovern KE, Clarke SC, et al. Global landscape of
590 HIV–human protein complexes. Nature. 2012 Jan 19;481(7381):365–70.

591 11. Martinez-Martin N, Marcandalli J, Huang CS, Arthur CP, Perotti M, Foglierini M, et al. An Unbiased
592 Screen for Human Cytomegalovirus Identifies Neuropilin-2 as a Central Viral Receptor. Cell. 2018
593 Aug;174(5):1158-1171.e19.

594 12. Gordon DE, Jang GM, Bouhaddou M, Xu J, Obernier K, White KM, et al. A SARS-CoV-2 protein
595 interaction map reveals targets for drug repurposing. Nature. 2020 Jul 16;583(7816):459–68.

596 13. Frei AP, Jeon O-Y, Kilcher S, Moest H, Henning LM, Jost C, et al. Direct identification of ligand-
597 receptor interactions on living cells and tissues. Nat Biotechnol. 2012 Oct;30(10):997–1001.

598 14. Sobotzki N, Schafroth MA, Rudnicka A, Koetemann A, Marty F, Goetze S, et al. HATRIC-based
599 identification of receptors for orphan ligands. Nat Commun. 2018 Dec;9(1):1519.

600 15. Srivastava M, Zhang Y, Chen J, Sirohi D, Miller A, Zhang Y, et al. Chemical proteomics tracks virus
601 entry and uncovers NCAM1 as Zika virus receptor. Nat Commun. 2020 Dec;11(1):3896.

602 16. Terracciano R, Preianò M, Fregola A, Pelaia C, Montalcini T, Savino R. Mapping the SARS-CoV-2–
603 Host Protein–Protein Interactome by Affinity Purification Mass Spectrometry and Proximity-Dependent
604 Biotin Labeling: A Rational and Straightforward Route to Discover Host-Directed Anti-SARS-CoV-2
605 Therapeutics. Int J Mol Sci. 2021 Jan 7;22(2):532.

606 17. Coyaud E, Ranadheera C, Cheng D, Gonçalves J, Dyakov BJA, Laurent EMN, et al. Global
607 Interactomics Uncovers Extensive Organellar Targeting by Zika Virus. Mol Cell Proteomics. 2018
608 Nov;17(11):2242–55.

609 18. Hauri S, Khakzad H, Happonen L, Teleman J, Malmström J, Malmström L. Rapid determination of
610 quaternary protein structures in complex biological samples. Nat Commun. 2019 Dec;10(1):192.

611 19. Chowdhury S, Khakzad H, Bergdahl GE, Lood R, Ekstrom S, Linke D, et al. Streptococcus pyogenes
612 Forms Serotype- and Local Environment-Dependent Interspecies Protein Complexes. mSystems. 2021 Oct
613 26;6(5):e0027121.

614 20. Kupča AM, Essbauer S, Zoeller G, de Mendonça PG, Brey R, Rinder M, et al. Isolation and molecular
615 characterization of a tick-borne encephalitis virus strain from a new tick-borne encephalitis focus with
616 severe cases in Bavaria, Germany. Ticks Tick-Borne Dis. 2010 Mar;1(1):44–51.

617 21. Han X, Juceviciene A, Uzcategui NY, Brummer-Korvenkontio H, Zygutiene M, Jääskeläinen A, et al.
618 Molecular epidemiology of tick-borne encephalitis virus inIxodes ricinus ticks in Lithuania. J Med Virol. 2005
619 Oct;77(2):249–56.

620 22. Bogovic P. Tick-borne encephalitis: A review of epidemiology, clinical characteristics, and
621 management. World J Clin Cases. 2015;3(5):430.

622 23. Taba P, Schmutzhard E, Forsberg P, Lutsar I, Ljøstad U, Mygland Å, et al. EAN consensus review on
623 prevention, diagnosis and management of tick-borne encephalitis. Eur J Neurol. 2017 Oct;24(10):1214-e61.

624 24. Füzik T, Formanová P, Růžek D, Yoshii K, Niedrig M, Plevka P. Structure of tick-borne encephalitis
625 virus and its neutralization by a monoclonal antibody. Nat Commun. 2018 Dec;9(1):436.

626 25. Rey FA, Heinz FX, Mandl C, Kunz C, Harrison SC. The envelope glycoprotein from tick-borne
627 encephalitis virus at 2 Å resolution. Nature. 1995 May;375(6529):291–8.

628 26. Mandl CW, Allison SL, Holzmann H, Meixner T, Heinz FX. Attenuation of Tick-Borne Encephalitis
629 Virus by Structure-Based Site-Specific Mutagenesis of a Putative Flavivirus Receptor Binding Site. J Virol.
630 2000 Oct 15;74(20):9601–9.

631 27. Renner M, Dejnirattisai W, Carrique L, Martin IS, Karia D, Ilca SL, et al. Flavivirus maturation leads to
632 the formation of an occupied lipid pocket in the surface glycoproteins. Nat Commun. 2021 Dec;12(1):1238.

633 28. Chen Z-L, Meng J-M, Cao Y, Yin J-L, Fang R-Q, Fan S-B, et al. A high-speed search engine pLink 2 with
634 systematic evaluation for proteome-scale identification of cross-linked peptides. Nat Commun. 2019
635 Dec;10(1):3404.

636 29. Ma L, Jones CT, Groesch TD, Kuhn RJ, Post CB. Solution structure of dengue virus capsid protein
637 reveals another fold. Proc Natl Acad Sci. 2004 Mar 9;101(10):3414–9.

638 30. Dokland T, Walsh M, Mackenzie JM, Khromykh AA, Ee K-H, Wang S. West Nile Virus Core Protein.
639 Structure. 2004 Jul;12(7):1157–63.

640 31. Shang Z, Song H, Shi Y, Qi J, Gao GF. Crystal Structure of the Capsid Protein from Zika Virus. J Mol
641 Biol. 2018 Mar;430(7):948–62.

642 32. Zybailov BL. Large Scale Chemical Cross-linking Mass Spectrometry Perspectives. J Proteomics
643 Bioinform [Internet]. 2013 [cited 2021 Jun 10];01(S2). Available from: https://www.omicsonline.org/large-
644 scale-chemical-cross-linking-mass-spectrometry-perspectives-jpb.S2-001.php?aid=12235

645 33. Rinner O, Seebacher J, Walzthoeni T, Mueller LN, Beck M, Schmidt A, et al. Identification of cross-
646 linked peptides from large sequence databases. Nat Methods. 2008 Apr;5(4):315–8.

647 34. Roy A, Kucukural A, Zhang Y. I-TASSER: a unified platform for automated protein structure and
648 function prediction. Nat Protoc. 2010 Apr;5(4):725–38.

649 35. Yang J, Yan R, Roy A, Xu D, Poisson J, Zhang Y. The I-TASSER Suite: protein structure and function
650 prediction. Nat Methods. 2015 Jan;12(1):7–8.

651 36. Yang J, Zhang Y. I-TASSER server: new development for protein structure and function predictions.
652 Nucleic Acids Res. 2015 Jul 1;43(W1):W174–81.

653 37. Merkley ED, Rysavy S, Kahraman A, Hafen RP, Daggett V, Adkins JN. Distance restraints from
654 crosslinking mass spectrometry: Mining a molecular dynamics simulation database to evaluate lysine-lysine
655 distances: Evaluating Lysine-Lysine Distances by MD for XL-MS. Protein Sci. 2014 Jun;23(6):747–59.

656 38. Yang B, Wu Y-J, Zhu M, Fan S-B, Lin J, Zhang K, et al. Identification of cross-linked peptides from
657 complex samples. Nat Methods. 2012 Sep;9(9):904–6.

658 39. Debelyy MO, Waridel P, Quadroni M, Schneiter R, Conzelmann A. Chemical crosslinking and mass
659 spectrometry to elucidate the topology of integral membrane proteins. Gasset M, editor. PLOS ONE. 2017
660 Oct 26;12(10):e0186840.

661 40. Szklarczyk D, Gable AL, Lyon D, Junge A, Wyder S, Huerta-Cepas J, et al. STRING v11: protein–
662 protein association networks with increased coverage, supporting functional discovery in genome-wide
663 experimental datasets. Nucleic Acids Res. 2019 Jan 8;47(D1):D607–13.

664 41. Yuan S, Liu Z, Xu Z, Liu J, Zhang J. High mobility group box 1 (HMGB1): a pivotal regulator of
665 hematopoietic malignancies. J Hematol OncolJ Hematol Oncol. 2020 Dec;13(1):91.

666 42. Pokidysheva E, Zhang Y, Battisti AJ, Bator-Kelly CM, Chipman PR, Xiao C, et al. Cryo-EM
667 Reconstruction of Dengue Virus in Complex with the Carbohydrate Recognition Domain of DC-SIGN. Cell.
668 2006 Feb;124(3):485–93.

669 43. Jones AX, Cao Y, Tang Y-L, Wang J-H, Ding Y-H, Tan H, et al. Improving mass spectrometry analysis
670 of protein structures with arginine-selective chemical cross-linkers. Nat Commun. 2019 Dec;10(1):3911.

671 44. Leitner A, Joachimiak LA, Unverdorben P, Walzthoeni T, Frydman J, Förster F, et al. Chemical cross-
672 linking/mass spectrometry targeting acidic residues in proteins and protein complexes. Proc Natl Acad Sci.
673 2014 Jul 1;111(26):9455–60.

674 45. Malygin AA, Bondarenko EI, Ivanisenko VA, Protopopova EV, Karpova GG, Loktev VB. C-terminal
675 fragment of human laminin-binding protein contains a receptor domain for Venezuelan equine encephalitis
676 and tick-borne encephalitis viruses. Biochem Mosc. 2009 Dec;74(12):1328–36.

677 46. Protopopova EV, Sorokin AV, Konovalova SN, Kachko AV, Netesov SV, Loktev VB. Human laminin
678 binding protein as a cell receptor for the tick-borne encephalitis virus. Zentralblatt Für Bakteriol. 1999
679 Dec;289(5–7):632–8.

680 47. Maginnis MS, Forrest JC, Kopecky-Bromberg SA, Dickeson SK, Santoro SA, Zutter MM, et al. β1
681 Integrin Mediates Internalization of Mammalian Reovirus. J Virol. 2006 Mar 15;80(6):2760–70.

682 48. Feire AL, Roy RM, Manley K, Compton T. The Glycoprotein B Disintegrin-Like Domain Binds Beta 1
683 Integrin To Mediate Cytomegalovirus Entry. J Virol. 2010 Oct;84(19):10026–37.

684 49. Xiao J, Palefsky JM, Herrera R, Berline J, Tugizov SM. The Epstein–Barr virus BMRF-2 protein
685 facilitates virus attachment to oral epithelial cells. Virology. 2008 Jan;370(2):430–42.

686 50. Weigel-Kelley KA, Yoder MC, Srivastava A. α5β1 integrin as a cellular coreceptor for human
687 parvovirus B19: requirement of functional activation of β1 integrin for viral entry. Blood. 2003 Dec
688 1;102(12):3927–33.

689 51. Liu X, Li F, Zhang J, Wang L, Wang J, Wen Z, et al. The ATPase ATP6V1A facilitates rabies virus
690 replication by promoting virion uncoating and interacting with the viral matrix protein. J Biol Chem. 2021
691 Jan;296:100096.

692 52. Liu Y-G, Chen Y, Wang X, Zhao P, Zhu Y, Qi Z. Ezrin is essential for the entry of Japanese encephalitis
693 virus into the human brain microvascular endothelial cells. Emerg Microbes Infect. 2020 Jan 1;9(1):1330–
694 41.

695 53. Liu Q, Huang X, Zhao D, Han K, Liu Y, Yang J, et al. Identification of heat shock protein A9 as a
696 Tembusu virus binding protein on DF-1 cells. Virus Res. 2017 Jan;227:110–4.

697 54. Jindadamrongwech S, Thepparit C, Smith DR. Identification of GRP 78 (BiP) as a liver cell expressed
698 receptor element for dengue virus serotype 2. Arch Virol. 2004 May;149(5):915–27.

699 55. Khongwichit S, Sornjai W, Jitobaom K, Greenwood M, Greenwood MP, Hitakarun A, et al. A
700 functional interaction between GRP78 and Zika virus E protein. Sci Rep. 2021 Jan 11;11(1):393.

701 56. Nain M, Mukherjee S, Karmakar SP, Paton AW, Paton JC, Abdin MZ, et al. GRP78 Is an Important
702 Host Factor for Japanese Encephalitis Virus Entry and Replication in Mammalian Cells. J Virol. 2017 Mar
703 15;91(6):e02274-16.

704 57. Zhao D, Liu Q, Han K, Wang H, Yang J, Bi K, et al. Identification of Glucose-Regulated Protein 78
705 (GRP78) as a Receptor in BHK-21 Cells for Duck Tembusu Virus Infection. Front Microbiol. 2018 Apr 9;9:694.

706 58. Dana RC, Welch WJ, Deftos LJ. Heat shock proteins bind calcitonin. Endocrinology. 1990
707 Jan;126(1):672–4.

708 59. Oka OBV, Pringle MA, Schopp IM, Braakman I, Bulleid NJ. ERdj5 is the ER reductase that catalyzes
709 the removal of non-native disulfides and correct folding of the LDL receptor. Mol Cell. 2013 Jun
710 27;50(6):793–804.

711 60. Evensen NA, Kuscu C, Nguyen H-L, Zarrabi K, Dufour A, Kadam P, et al. Unraveling the role of
712 KIAA1199, a novel endoplasmic reticulum protein, in cancer cell migration. J Natl Cancer Inst. 2013 Sep
713 18;105(18):1402–16.

714 61. Cuevas EP, Eraso P, Mazón MJ, Santos V, Moreno-Bueno G, Cano A, et al. LOXL2 drives epithelial-
715 mesenchymal transition via activation of IRE1-XBP1 signalling pathway. Sci Rep. 2017 Mar 23;7:44988.

716 62. Bellani S, Mescola A, Ronzitti G, Tsushima H, Tilve S, Canale C, et al. GRP78 clustering at the cell
717 surface of neurons transduces the action of exogenous alpha-synuclein. Cell Death Differ. 2014
718 Dec;21(12):1971–83.

719 63. Bhattacharjee G, Ahamed J, Pedersen B, El-Sheikh A, Mackman N, Ruf W, et al. Regulation of tissue
720 factor--mediated initiation of the coagulation cascade by cell surface grp78. Arterioscler Thromb Vasc Biol.
721 2005 Aug;25(8):1737–43.

722 64. Philippova M, Ivanov D, Joshi MB, Kyriakakis E, Rupp K, Afonyushkin T, et al. Identification of
723 Proteins Associating with Glycosylphosphatidylinositol- Anchored T-Cadherin on the Surface of Vascular
724 Endothelial Cells: Role for Grp78/BiP in T-Cadherin-Dependent Cell Survival. Mol Cell Biol. 2008 Jun
725 15;28(12):4004–17.

726 65. Honda T, Horie M, Daito T, Ikuta K, Tomonaga K. Molecular Chaperone BiP Interacts with Borna
727 Disease Virus Glycoprotein at the Cell Surface. J Virol. 2009 Dec;83(23):12622–5.

728 66. Mayer MP, Gierasch LM. Recent advances in the structural and mechanistic aspects of Hsp70
729 molecular chaperones. J Biol Chem. 2019 Feb;294(6):2085–97.

730 67. Elfiky AA, Ibrahim IM. Zika virus envelope – heat shock protein A5 (GRP78) binding site prediction. J
731 Biomol Struct Dyn. 2021 Sep 22;39(14):5248–60.

732 68. van der Schaar HM, Rust MJ, Chen C, van der Ende-Metselaar H, Wilschut J, Zhuang X, et al.
733 Dissecting the Cell Entry Pathway of Dengue Virus by Single-Particle Tracking in Living Cells. Farzan M,
734 editor. PLoS Pathog. 2008 Dec 19;4(12):e1000244.

735 69. Suksanpaisan L, Susantad T, Smith DR. Characterization of dengue virus entry into HepG2 cells. J
736 Biomed Sci. 2009;16(1):17.

737 70. Iacono-Connors LC, Smith JF, Ksiazek TG, Kelley CL, Schmaljohn CS. Characterization of Langat virus
738 antigenic determinants defined by monoclonal antibodies to E, NS1 and preM and identification of a
739 protective, non-neutralizing preM-specific monoclonal antibody. Virus Res. 1996 Aug;43(2):125–36.

740 71. Teleman J, Dowsey AW, Gonzalez-Galarza FF, Perkins S, Pratt B, Röst HL, et al. Numerical
741 Compression Schemes for Proteomics Mass Spectrometry Data. Mol Cell Proteomics. 2014 Jun;13(6):1537–
742 42.

743 72. Chambers MC, Maclean B, Burke R, Amodei D, Ruderman DL, Neumann S, et al. A cross-platform
744 toolkit for mass spectrometry and proteomics. Nat Biotechnol. 2012 Oct;30(10):918–20.

745 73. Bauch A, Adamczyk I, Buczek P, Elmer F-J, Enimanev K, Glyzewski P, et al. openBIS: a flexible
746 framework for managing and analyzing complex data in biology research. BMC Bioinformatics.
747 2011;12(1):468.

748 74. Craig R, Beavis RC. A method for reducing the time required to match protein sequences with
749 tandem mass spectra. Rapid Commun Mass Spectrom. 2003 Oct 30;17(20):2310–6.

750 75. Geer LY, Markey SP, Kowalak JA, Wagner L, Xu M, Maynard DM, et al. Open Mass Spectrometry
751 Search Algorithm. J Proteome Res. 2004 Oct;3(5):958–64.

752 76. Eng JK, Jahan TA, Hoopmann MR. Comet: An open-source MS/MS sequence database search tool.
753 PROTEOMICS. 2013 Jan;13(1):22–4.

754 77. Keller A, Nesvizhskii AI, Kolker E, Aebersold R. Empirical Statistical Model To Estimate the Accuracy
755 of Peptide Identifications Made by MS/MS and Database Search. Anal Chem. 2002 Oct 1;74(20):5383–92.

756 78. Reiter L, Claassen M, Schrimpf SP, Jovanovic M, Schmidt A, Buhmann JM, et al. Protein
757 Identification False Discovery Rates for Very Large Proteomics Data Sets Generated by Tandem Mass
758 Spectrometry. Mol Cell Proteomics. 2009 Nov;8(11):2405–17.

759 79. Pettersen EF, Goddard TD, Huang CC, Couch GS, Greenblatt DM, Meng EC, et al. UCSF Chimera?A
760 visualization system for exploratory research and analysis. J Comput Chem. 2004 Oct;25(13):1605–12.

761 80. Shannon P. Cytoscape: A Software Environment for Integrated Models of Biomolecular Interaction
762 Networks. Genome Res. 2003 Nov 1;13(11):2498–504.

763 81. Pomaznoy M, Ha B, Peters B. GOnet: a tool for interactive Gene Ontology analysis. BMC
764 Bioinformatics. 2018 Dec;19(1):470.

765 Supporting information captions

766 **S1 Table: DDA analysis of viral and host protein in all samples** (XLSX).

767 **S2 Table: Cross-linking dataset** Identified cross-linked peptides, corresponding proteins, E-values and SVM
768 scores for each cross-linked spectral observation (XLSX).

769 **S3 Table: Filtered cross-linking dataset** Cross-linking dataset (S2 Table) filtered to remove spectral
770 observations corresponding to unique cross-links identified by less than 2 spectral observations with SVM
771 scores < 0.355 (XLSX).

772 **S4 Table: GO analysis of host proteins** GO analysis of the 59 host proteins shown to interact with the
773 surface of TBEV in the filtered cross-linking dataset (S3 Table) (XLSX).

774 **S1 File: Correlation between number of cross-linked spectral observations, protein abundance and**
775 **protein lysine content** Table showing the number of cross-linked spectral observations, the average protein
776 abundance calculated in the DDA analysis (S1 Table) and the number of lysines for 101 randomly selected
777 proteins. Scatter graphs show no correlation between the number of cross-linked spectral observations and
778 the number of lysines for the proteins, and no correlation between the number of cross-linked spectral
779 observations and the protein abundance (XLSX).

780 **S1 Fig: Box and whisker plot of the E-value for the intraviral cross-links, plotted against the distance**
781 **between the cross-linked residues for each cross-link.** The smallest distance out of the mature and
782 immature calculated distances, and the C protein dimer or monomer distances is plotted. The mean E-value
783 is marked with a cross.